ARTICLES
PUBLISHED ONLINE: 12 FEBRUARY 2012 | DOI: 10.1038/NNANO.2012.3
nature nanotechnology

Oral exposure to polystyrene nanoparticles affects iron absorption

Gretchen J. Mahler[1], Mandy B. Esch[2], Elad Tako[3], Teresa L. Southard[4], Shivaun D. Archer[2], Raymond P. Glahn[3] and Michael L. Shuler[2]*

The use of engineered nanoparticles in food and pharmaceuticals is expected to increase, but the impact of chronic oral exposure to nanoparticles on human health remains unknown. Here, we show that chronic and acute oral exposure to polystyrene nanoparticles can influence iron uptake and iron transport in an *in vitro* model of the intestinal epithelium and an *in vivo* chicken intestinal loop model. Intestinal cells that are exposed to high doses of nanoparticles showed increased iron transport due to nanoparticle disruption of the cell membrane. Chickens acutely exposed to carboxylated particles (50 nm in diameter) had a lower iron absorption than unexposed or chronically exposed birds. Chronic exposure caused remodelling of the intestinal villi, which increased the surface area available for iron absorption. The agreement between the *in vitro* and *in vivo* results suggests that our *in vitro* intestinal epithelium model is potentially useful for toxicology studies.

Engineered nanoparticles have unique physical and chemical properties and are currently used in a variety of applications, including the food[1–4] and pharmaceutical industries[5,6]. The increased surface area, unique crystalline structure, small size and enhanced reactivity of some nanomaterials, however, may lead to harmful interactions with cellular material, and no studies have addressed the chronic effects of nanoparticle exposure on the normal function of the intestinal epithelium[7].

It is estimated that the average person in a developed country consumes between 10^{12} and 10^{14} man-made fine (diameter, 0.1–1 μm) to ultrafine (diameter, <100 nm) particles every day[8]. These dietary particles are mainly TiO_2, silicates and aluminosilicates derived from food additives such as stabilizers and anticaking agents[8]. Because most of these micro- and nanoparticles have negatively charged surfaces, they can bind to biomolecules in the gut lumen, absorb across the gastrointestinal tract and accumulate at the base of Peyer's patches, where a large concentration of M cells are found[8]. M cells transport microorganisms and particles from the gut lumen to immune cells across the intestinal epithelium, and are important for defending the body against ingested toxic substances and stimulating mucosal immunity[9].

The ingestion of dietary particles has been thought to promote the development of Crohn's disease, which is characterized by transmural inflammation of the gastrointestinal tract that first appears over the Peyer's patches[10]. Lomer *et al.* have shown that patients with Crohn's disease who followed a diet low in TiO_2 and aluminosilicate microparticles for four months had a reduction in the Crohn's disease activity index[10]. Patients with Crohn's disease are also prone to iron deficiency, suggesting a possible link between nanoparticle consumption, the development of Crohn's disease and iron absorption[11].

Oral delivery is the preferred route of pharmaceutical administration because it is inexpensive, non-invasive and convenient for patients[12]. Polymeric nanoparticle carriers are useful for drug delivery because they are more stable than other colloidal carriers in the gastrointestinal tract and, compared to their micrometre-sized counterparts, the diameter to surface area ratio of nanoparticles favours absorption through the intestinal epithelium[13]. Furthermore, the physical and chemical characteristics, drug release profile and biological behaviour of polymeric nanoparticles can be manipulated easily[14]. Although many potential peptide and protein therapeutics will be administered at least daily, very little is known about the chronic effects of nanoparticle ingestion.

The goal of this work was to investigate the effects of oral exposure to nanoparticles on the absorption of iron. Using a physiologically realistic *in vitro* model of the intestinal epithelium and *in vivo* chicken intestinal loop model, we showed that acute exposure to 50 nm polystyrene carboxylated nanoparticles can inhibit iron transport. In chronically exposed chickens, the 50 nm carboxylated particles caused a remodelling of the intestinal villi to increase the surface area available for iron absorption. We chose iron absorption as a subject because iron is an example of an essential nutrient that is transported across the intestinal epithelium by means of complex, highly regulated, protein-assisted vesicular and non-vesicular mechanisms[15]. The polystyrene nanoparticles used in this study (particle characterization shown in Table 1) were chosen as a model particle to demonstrate that our *in vitro* and *in vivo* experimental systems can be used for evaluating the subtle effects of nanoparticle consumption.

Nanoparticle dose calculations

In vitro and *in vivo* doses of nanoparticles were formulated to mimic potential human exposure. The total surface area of the human small intestine is 2×10^6 cm^2, and the duodenum, which is the first section of the small intestine and the site where most iron absorption occurs, has ~900 cm^2 of absorbing surface area[16–18]. If 10^{14} particles are ingested, this represents a dose of 10^7 particles per cm^2 to the small intestine. If 10^{12} or 10^{14} particles are ingested, the dose to the duodenum is $\sim 10^9$ or $\sim 10^{11}$ particles per cm^2, respectively. If 0.02 mg kg^{-1} of 50 nm polystyrene particles were administered to a 70 kg human as a pharmaceutical, the dose to the small intestine would be 10^7 particles per cm^2 assuming that

[1]Department of Bioengineering, Binghamton University, Binghamton, New York 13902, USA, [2]Department of Biomedical Engineering, Cornell University, Ithaca, New York 14853, USA, [3]Plant, Soil and Nutrition Laboratory, Agricultural Research Services, US Department of Agriculture, Tower Road, Ithaca, New York 14853, USA, [4]Department of Biomedical Sciences, Cornell University, Ithaca, New York 14853, USA. *e-mail: mls50@cornell.edu

Table 1 | Nanoparticle characterization.

Particle	Measured diameter ($n = 6$)	Surface area (calculated)	Functional groups	ζ in water (mV)	ζ in MEM (mV)
50 nm carboxylated	40 nm±7 nm	65,450 nm^3	-COOH	−60.0±5.9	−12.2±0.7
200 nm carboxylated	209 nm±2 nm	4,188,790 nm^3	-COOH	−60.2±5.1	−17.3±0.4
50 nm non-ionized	38 nm±5 nm	65,450 nm^3		−39.5±2.9	−16.4±0.8
200 nm non-ionized	205 nm±1 nm	4,188,790 nm^3		−43.9±1.9	−17.3±0.3
50 nm aminated	34 nm±2 nm	65,450 nm^3	$-NH_2$	27.1±2.1	−6.2±0.3
200 nm aminated	197 nm±5 nm	4,188,790 nm^3	$-NH_2$	10.5±1.8	−9.2±0.2

the particles are monodispersed and have a density of 1.053 g cm^{-3} (ref. 19). Oral administrations of 2 mg kg^{-1} and 200 mg kg^{-1} oral would translate to doses of 10^9 and 10^{11} particles per cm^2 to the small intestine, respectively.

The doses of 50 nm particles applied to the cell cultures used in this study (assuming that the presence of microvilli increases the surface area by a factor of 20; ref. 16), were 10^7, 10^9 and 10^{11} particles per cm^2 for the low (2×10^9 particles per ml), medium (2×10^{11} particles per ml) and high (2×10^{13} particles per ml) experimental concentrations used. The doses of 200 nm particles (1.25×10^8 particles per ml, 1.25×10^{10} particles per ml and 1.25×10^{12} particles per ml) were determined by calculating the total surface area of particles in the 50 nm particle dose and normalizing the 200 nm particle dose by surface area. For *in vivo* experiments, chickens were given 2 mg kg^{-1} doses of carboxylated nanoparticles. A 2 mg kg^{-1} dose to a 3 kg chicken exposes the duodenum to 10^9 particles per cm^2 of surface area (the chicken duodenum is the primary site of iron absorption)[20]. The surface area of the chicken duodenum was estimated to be ~1,600 cm^2 based on previously published values[21–24], and the effective surface area of the duodenum was estimated to be 15 times that value, or ~24,000 cm^2, due to the presence of 10^5 microvilli per villi[25].

In vitro model characterization

Our *in vitro* model of the intestinal epithelium mimics the absorptive enterocytes, goblet cells and M cells that populate the human small-intestinal lining. Absorptive enterocytes and mucus-producing goblet cells are the two most common cell types in the intestinal epithelium[18]. Caco-2 cells absorb and transport iron, mimicking absorptive enterocytes, and HT29-MTX mucus-secreting cells mimic goblet cells[26,27]. We have shown that co-cultures of Caco-2 and HT29-MTX have a mucus layer that completely covers the cell monolayer[28]. Culturing Caco-2 monolayers in the proximity of the Raji B lymphocyte cell line induces Caco-2 differentiation into cells with an M cell-like morphology[9]. M cells are known to express a greater amount of β1-integrin on the apical surface, and sialyl Lewis A antigen has been shown by Giannasca *et al.* to distinguish human M cells from other intestinal epithelial cell types[29,30]. Supplementary Fig. 1 presents a diagram of the culture conditions for the Caco-2/HT29-MTX (co-cultures of Caco-2 and HT29-MTX) and +M cell (tri-cultures of Caco-2, HT29-MTX and Raji B) monolayers. Supplementary Fig. 2 shows the increased β1-integrin expression on the apical side of +M cell monolayers, and sialyl Lewis A antigen expression in +M cell monolayers can be seen in Supplementary Fig. 3. Image analysis of sialyl Lewis A antigen staining reveals that the tricultures have an average of 2.55% (±0.29%) differentiated M cells. This compares well with human physiology, as the human small-intestinal epithelial membrane has fewer than 10% M cells[31]. Figure 1a shows +M cell monolayers after exposure to 50 nm particles, and Fig. 1b and Supplementary Fig. 4 show +M cell monolayers after exposure to 200 nm particles. The 50 nm particles are localized at the cell membrane, but more vesicles can be seen in monolayers exposed to 200 nm particles.

Caco-2/HT29-MTX and +M cell monolayers were exposed to a medium dose of 50 nm or 200 nm particles at 4 °C and 37 °C to determine if the particles were transported by an energy-dependent process. After 45 min, Caco-2/HT29-MTX monolayers transported 4.32×10^8 50 nm particles at 4 °C and 4.63×10^8 at 37 °C. However, +M cell monolayers transported 4.92×10^8 50 nm particles at 4 °C and 6.15×10^8 at 37 °C (Fig. 2a). After 45 min, the Caco-2/HT29-MTX monolayers transported no 200 nm particles at 4 °C and 1.06×10^6 at 37 °C, and the +M cell monolayers transported 7.37×10^5 of the 200 nm particles at 4 °C and 7.38×10^6 at 37 °C after the same period (Fig. 2b). Taken together, these results

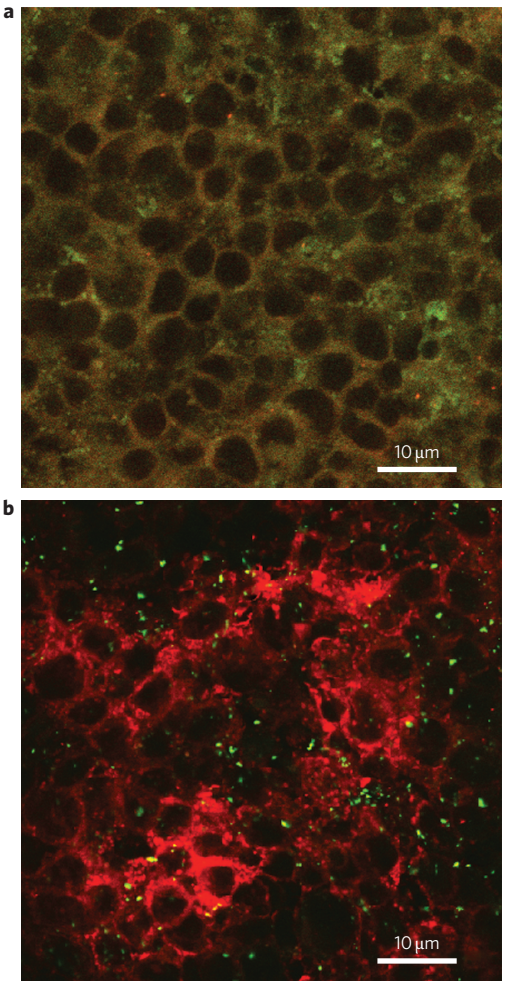

Figure 1 | *In vitro* +M cells monolayer after exposure to carboxylated polystyrene nanoparticles. a, +M cell monolayer stained with CellTracker CM-DiI cell membrane stain (red) after 4 h exposure to 50 nm carboxylated polystyrene nanoparticles (green) at 2×10^{11} particles per ml. The green particles and red cell membranes overlap, showing that the hydrophobic polystyrene particles primarily diffuse through hydrophobic cell membranes. **b**, +M cells monolayer stained with CM-DiI stain (red) after 4 h exposure to 200 nm carboxylated polystyrene particles (green) at 1.25×10^{10} particles per ml. More vesicles (red) can be seen than in +M cell monolayers exposed to 50 nm particles.

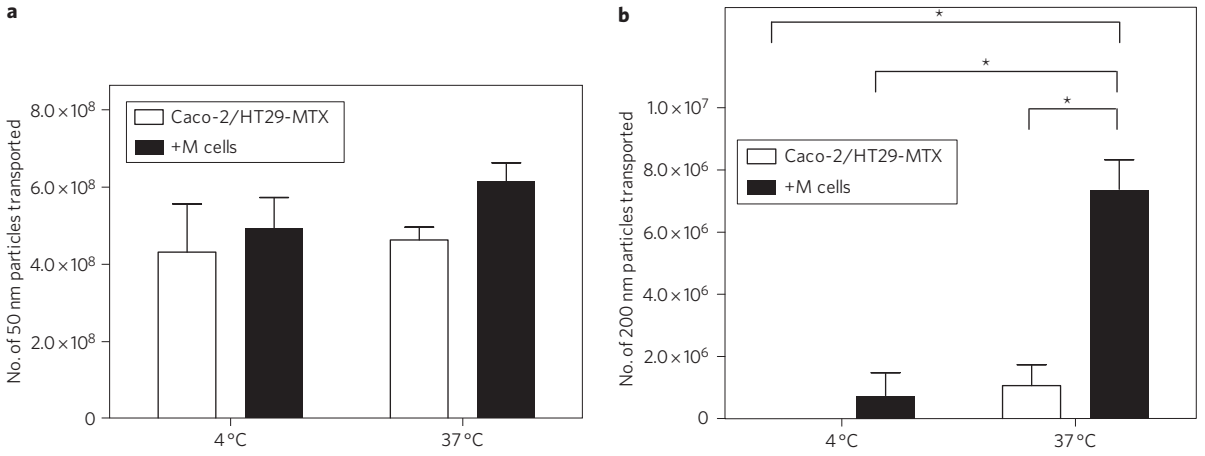

Figure 2 | Particle transport experiments at 4 °C and 37 °C. a, Caco-2/HT29-MTX and +M cell monolayers exposed to 2×10^{11} 50 nm carboxylated particles per ml at 4 °C and 37 °C did not show any significant differences in particle transport, suggesting that 50 nm particles are passively transported through the monolayers using a paracellular, non-energy-dependent process. **b**, Caco-2/HT29-MTX and +M cells monolayers exposed to 1.25×10^{10} 200 nm carboxylated particles per ml at 4 °C and 37 °C. Significantly more 200 nm particles were transported by the +M cell monolayer at 37 °C than the +M cell monolayer at 4 °C or the Caco2/HT29-MTX monolayer at 4 °C and 37 °C. This suggests that 200 nm particles are transported primarily through energy-dependent mechanisms such as within cellular vesicles. Error bars, ±s.e.m. Mean particle transport differences between Caco-2/HT29-MTX monolayers at 4 °C and 37 °C and +M cell monolayers at 4 °C and 37 °C that are significant according to a one-way ANOVA with Tukey's post test are indicated with an asterisk ($P < 0.05$, $n = 3$).

show that the transport of 50 nm particles is predominately a paracellular, non-energy-dependent process, but the 200 nm particles are primarily transported via energy-dependent mechanisms, such as within cellular vesicles.

Nanoparticle exposure disrupts iron transport *in vitro*

The *in vitro* experimental set-up is shown in Fig. 3a. Cell monolayers were grown on Transwell inserts. Iron uptake was quantified by the amount of ^{59}Fe within the cell monolayers, and iron transport as the amount of ^{59}Fe that crossed the model epithelium and reached the culture medium in the bottom Transwell chamber. The results for iron uptake and iron transport following a 4 h exposure to low, medium or high concentrations of carboxylated nanoparticles are shown in Fig. 3b–g and are expressed as a percent increase or decrease compared to controls. Controls were corresponding Caco-2/HT29-MTX or +M cell monolayers that were not exposed to the particles.

High doses of 50 nm nanoparticles significantly increased the iron uptake and transport in Caco-2/HT29-MTX and +M cell monolayer (Fig. 3b,c). High doses of 200 nm nanoparticles significantly decreased Caco-2/HT29-MTX iron uptake, and significantly increased iron transport in Caco-2/HT29-MTX and +M cell monolayers (Fig. 3b,c). At medium doses of carboxylated particles, iron uptake from the solution was not affected, but 50 nm particles caused a significant decrease in iron transport through the Caco-2/HT29-MTX monolayers and 200 nm particles caused a significant decrease in iron transport through +M cell monolayers (Fig. 3d,e). Low doses of 50 and 200 nm particles did not affect iron uptake or transport (Fig. 3f,g). These results shown that iron transport (which is representative of *in vivo* iron transfer into the bloodstream) and iron uptake (which measures the amount of iron taken up by the cell) are differentially sensitive to particle exposure at realistic food or pharmaceutical doses.

Staining for the tight junctional protein occludin and measuring the transepithelial resistance (TER) are two common methods for evaluating epithelial monolayer integrity and tight junction functionality[32,33]. An increase in tight junction permeability is considered a sublethal toxic effect as it disrupts the barrier function of the intestinal epithelium and allows molecules to flow freely from the intestinal lumen to the blood circulation[33]. The TER of Caco-2 and +M cell monolayers was significantly decreased after exposure to high doses of 50 or 200 nm particles (Supplementary Fig. 6a,b). A decrease in TER indicates that high doses of particles were increasing the permeability of the tight junctions and allowing more iron to pass through. The TER values of monolayers exposed to low or medium doses of 50 or 200 nm particles were not significantly different from unexposed controls (Supplementary Fig. 6a,b), and medium doses of 50 nm particles had no effect on occludin (Supplementary Fig. 5c). We speculate that the decrease in iron transport due to medium-dose 50 nm or 200 nm particle exposure is because of a mechanical disruption of the membrane-bound iron transport proteins by the particles.

The effects of nanoparticle charge at medium doses on iron uptake and transport are shown in Fig. 4. Non-ionized particles did not significantly affect iron uptake or transport (Fig. 4a,b). The +50 nm particles significantly increased Caco-2/HT29-MTX and +M cell monolayer iron uptake and Caco-2/HT29-MTX iron transport, while the +200 nm particles did not have any effect on iron uptake and transport (Fig. 4c,d). Exposure to medium doses of +50 nm particles decreased the TER of Caco-2/HT29-MTX monolayers, and occludin staining showed weakened staining and disruption of the Caco-2/HT29-MTX monolayer tight junctional complexes (Supplementary Figs 5d and 6c,d). This agrees with previous work by Ranaldi and colleagues, which showed that polycationic compounds increased the permeability of Caco-2 tight junctions due to morphological changes in the F-actin cytoskeleton[33]. The increased iron uptake by monolayers exposed to +50 nm particles is probably due to the increased tight junction permeability, as increased transcytosis of luminal material often accompanies tight junction dysfunction[34,35].

Ferritin levels were analysed in all samples to exclude pre-existing differences in iron status as a cause for differences in iron transport or uptake. Ferritin levels in all nanoparticle-exposed and control cultures were not significantly different ($P < 0.05$).

Nanoparticle exposure affects iron transport *in vivo*

Adult broiler chickens were used for *in vivo* iron absorption studies. The chicken gastrointestinal tract has features similar to those of the human gastrointestinal tract, and we have recently shown that broiler chickens provide an accurate *in vivo* model for iron

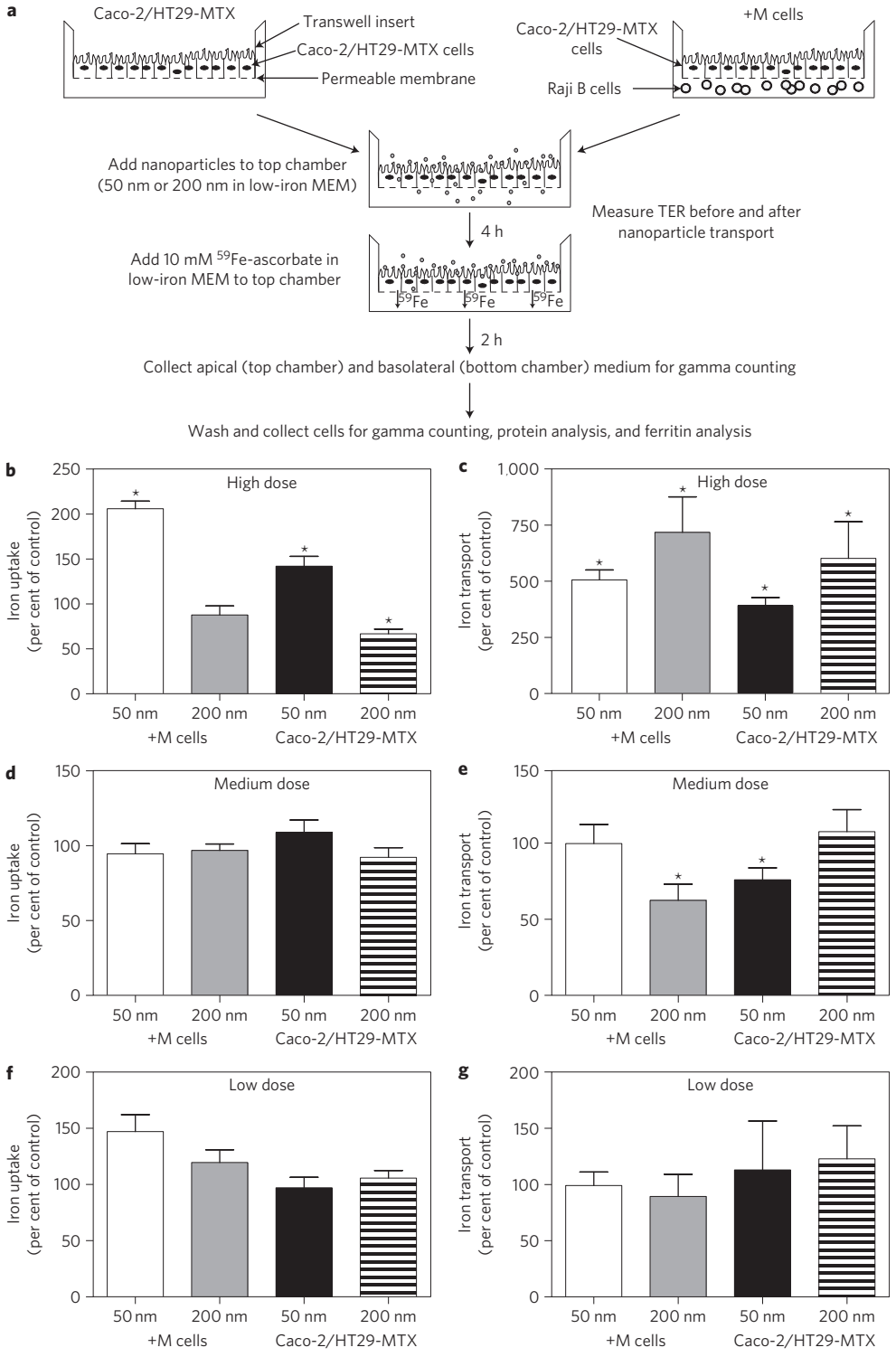

Figure 3 | *In vitro* iron uptake and transport results after exposure to carboxylated particles. a, *In vitro* experimental set-up. **b**–**g**, Iron uptake (**b**,**d**,**f**) and iron transport (**c**,**e**,**g**) after exposure to high (2×10^{13} 50 nm particles per ml or 1.25×10^{12} 200 nm particles per ml; **b**,**c**), medium (2×10^{11} 50 nm particles per ml or 1.25×10^{10} 200 nm particles per ml; **d**,**e**) or low (2×10^{9} 50 nm particles per ml or 1.25×10^{8} 200 nm particles per ml; **f**,**g**) doses of carboxylated particles. Results are expressed as per cent of control. Controls were Caco-2/HT29-MTX or +M cell monolayers that were not exposed to nanoparticles. Error bars, ±s.e.m. Differences in iron uptake or transport between +nanoparticle and control monolayers that are significant according to a one-way ANOVA with Tukey's post test are indicated with an asterisk ($P < 0.05$, $n = 6$).

bioavailability[36,37]. A timeline of the *in vivo* experimental procedure is shown in Fig. 5a. Starting at 6 weeks of age, chickens in the chronic exposure group were force-fed 2 mg kg^{-1} of 50 nm carboxylated polystyrene particles every morning for 2 weeks. The chronic exposure group was also given a 2 mg kg^{-1} dose of the 50 nm particles intraduodenually on the day of intestinal loop surgery. Birds in the acute exposure group were not exposed to nanoparticles until the day of intestinal loop surgery, at which

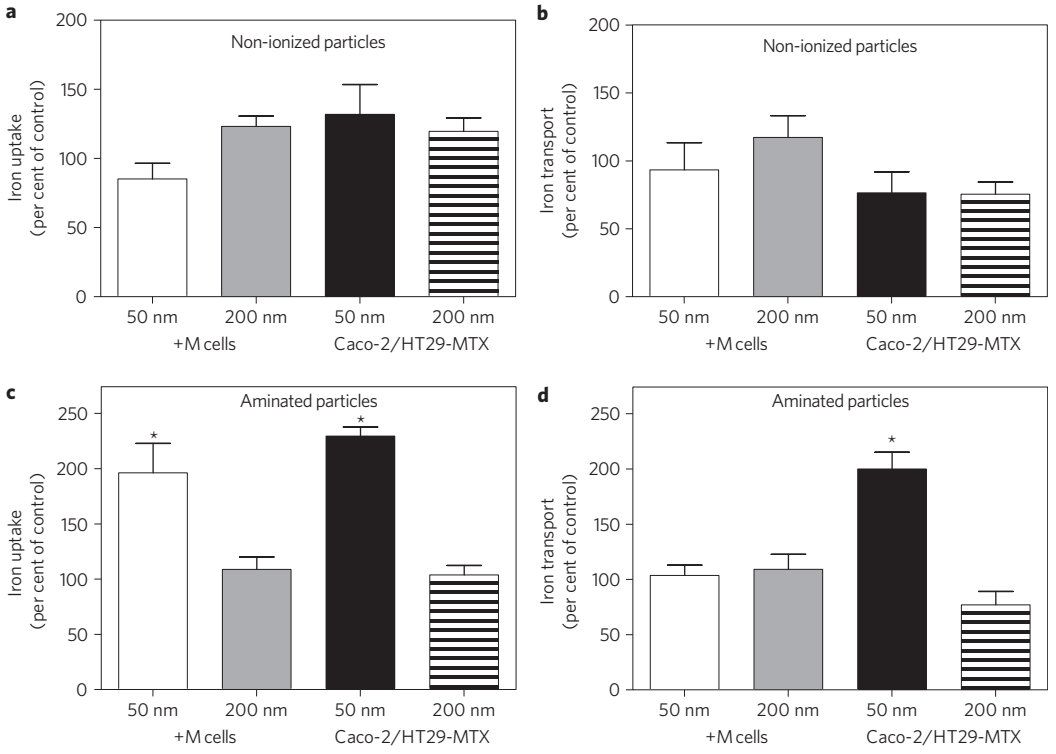

Figure 4 | *In vitro* iron uptake and transport results after exposure to non-ionized or aminated particles. a–d, Iron uptake (**a**,**c**) and iron transport (**b**,**d**) after exposure to non-ionized (**a**,**b**) or aminated (**c**,**d**) 50 nm or 200 nm particles at medium (2×10^{11} 50 nm particles per ml or 1.25×10^{10} 200 nm particles per ml) doses. Controls were Caco-2/HT29-MTX or +M cell monolayers that were not exposed to nanoparticles. Error bars, ±s.e.m. Differences in iron uptake or transport between +nanoparticle and control monolayers that are significant according to a one-way ANOVA with Tukey's post test are indicated with an asterisk ($P < 0.05$, $n = 6$).

point they were given a 2 mg kg^{-1} dose of 50 nm particles intraduodenually. The control group was not exposed to nanoparticles. Iron absorption was quantified by the amount of ^{58}Fe within the blood samples collected from the duodenal vein. On the day of intestinal loop surgery a ^{58}Fe-ascorbate solution (control group) or a ^{58}Fe-ascorbate solution containing a 2 mg kg^{-1} dose of 50 nm particles (chronic and acute groups) was injected intraduodenally, and the level of ^{58}Fe iron absorption was measured from duodenal vein blood samples. Ascorbic acid was added to the iron absorption solution as an iron absorption enhancer. Chickens in the acute exposure group had a significant decrease in iron absorption when compared with the control group birds, and chronic exposure group birds had a significant increase in iron absorption when compared with controls (Fig. 5b). Bird feed intakes, weights and haemoglobin levels were not significantly different between the treatment groups (Supplementary Table 2).

Supplementary Fig. 7 shows the zeta potential of the 50 nm particles in water, water with ^{58}Fe-ascorbate (the iron solution for *in vivo* experiments), minimal essential medium (MEM) and MEM with ^{56}Fe-ascorbate (the iron solution for *in vitro* experiments). ^{58}Fe-ascorbate slightly, but significantly, led to a decrease in the zeta potential of the nanoparticles in water, indicating some iron-particle binding. ^{56}Fe-ascorbate did not affect the zeta potential of the particles in MEM, most probably because proteins in the culture medium more effectively bind the charged particles. Supplementary Fig. 8 shows transmission electron microscopy images of the nanoparticles in MEM, and proteins (black dots) can be seen bound to the surface of the particles. The *in vivo* iron absorption data, which was performed with particles in water, is still valid because the iron and nanoparticle solution used for chronically and acutely exposed birds would have had an equal amount of iron trapping.

Liver ferritin levels[38,39] in the control, acute exposure and chronic exposure groups were not significantly different, suggesting that differences in iron status did not cause differences in iron transport (Fig. 5c). RNA was isolated from chicken duodenal samples to determine if transcript levels varied for DMT1, the apical iron transport protein, or NFKB1, a pro-inflammatory transcription factor[7,36]. Figure 5d shows that DMT1 and NFKB1 levels were not significantly different between the control, acute exposure and chronic exposure groups, demonstrating that the changes in iron absorption were not due to upregulation or downregulation of iron transport proteins or an inflammatory response. Further histological examination of the tissues showed that chickens in the chronic exposure group had more periportal accumulations of heterophils in the liver and a higher density of lymphoid follicles with active germinal centres in the spleens than chickens in the other groups (Supplementary Fig. 9). The differences seen in chickens from the chronic group may suggest mild immunostimulation.

Chicken duodenal samples were fixed in 10% formalin and sectioned transversely to visualize villi morphology. Villus surface area was calculated from villus height and an average of three villus width measurements[40,41]. Measurements of the villi showed that chronic exposure to nanoparticles significantly increased the overall villi volume (Fig. 5e). The intestinal structure can provide useful information about its function. Previous work has suggested that larger villi are capable of increased absorption of the available nutrients due to their greater absorptive surface area, the expression of brush border enzymes and nutrient transport systems[42,43]. Other work has shown that villus morphology is regulated by enteral nutrient absorption, but not intraluminal physical stimulation or parenterally delivered nutrition[44]. Overall, these *in vivo* experiments indicate that nanoparticle exposure causes a disruption in iron

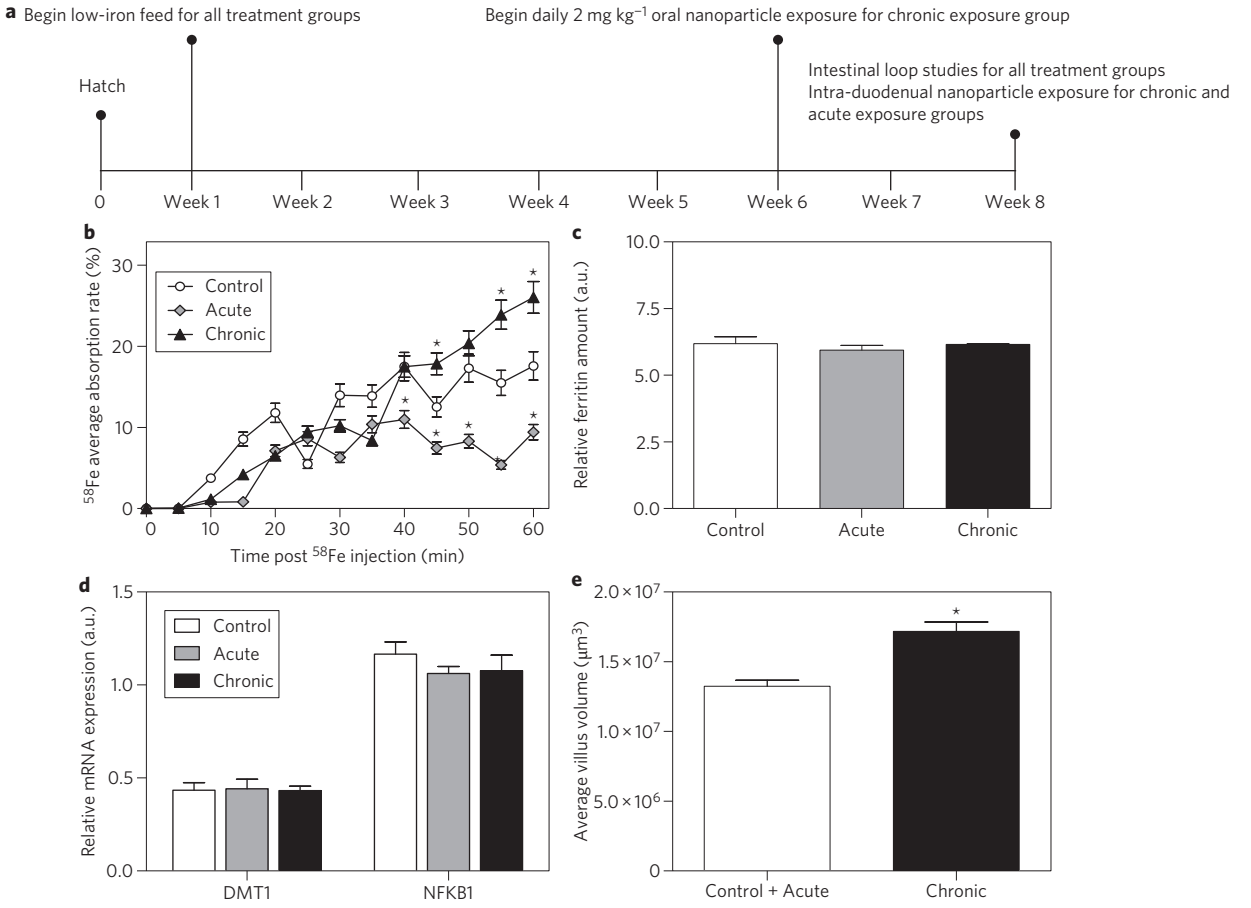

Figure 5 | *In vivo* iron transport, liver ferritin, gene expression and villus volume results. a, Timeline of chicken feeding schedule. **b**, Rate of iron absorption in the duodenal loop for control, acute and chronic exposure group chickens. Blood samples were collected before stable isotope injection and then every 5 min for 120 min post-solution injection. **c**,**d**, Liver ferritin (**c**) and duodenal DMT1 and NFKB1 transcript levels (**d**). In **d**, changes in mRNA expression were measured by semi-quantitative reverse transcription-polymerase chain reaction and expressed relative to the expression of 18S rRNA in arbitrary units (a.u.). **e**, Average duodenal villus volume. Error bars, ±s.e.m. For iron absorption, liver ferritin and mRNA expression, differences that are significantly different from the control group according to a one-way ANOVA with Tukey's post test are indicated with an asterisk ($P < 0.05$, $n = 3$ for the duodenal loop procedure; $n = 4$ for gene expression and ferritin evaluation). For average villus volume measurements, differences that are significant according to an unpaired Student's *t*-test are indicated with an asterisk. Differences were considered significant at $P < 0.05$.

transport and that the intestinal villi remodel to increase the surface area available for absorption. This increased area compensates for the disruption in iron transport caused by the nanoparticles.

Conclusions

The intestinal epithelial layer represents the initial gate that ingested nanoparticles must pass to reach the body. The polystyrene particles used in these experiments are generally considered non-toxic, but their interaction with a normal physiological process suggests a potential mechanism for a chronic, harmful, but subtle response. Similar disruptions in nutrient absorption could be possible in relation to other inorganic elements such as calcium, copper and zinc, which require passive or active transport systems for them to be absorbed through the intestinal epithelium. Fat-soluble vitamins such as vitamins A, D, E and K are absorbed only after micellization by pancreatic lipase[45]. Hydrophobic, charged nanoparticles could disrupt the formation of micelles, micelle interactions with the epithelial layer, and/or nutrient diffusion through the phospholipid membrane. An observation during the chicken surgeries was that the chronic exposure group birds' blood clotted more slowly than control or acute exposure group birds, and this could indicate a vitamin K deficiency[45].

In conclusion, we have shown, using cell culture and avian intestinal loop models of the intestinal epithelium, that acute oral exposure to polystyrene nanoparticles can disrupt iron transport and chronic exposure can cause remodelling of the intestinal villi. Remodelling of the villi increases the surface area available for iron absorption. Nanoparticle size, concentration and charge can influence iron uptake and iron transport at doses that represent potential human exposure. The increase in intestinal surface area compensated for the lowered iron transport caused by nanoparticle exposure. The consequences of oral nanoparticle exposure are largely unknown and more studies need to be performed on the effects of nanoparticles on nutrient absorption, especially in light of recent work showing that iron consumed from iron nanocompounds increases iron bioavailability[46]. Results measuring the effects of nanoparticle exposure on iron absorption obtained with our *in vitro* model of the intestinal epithelium corresponded well with *in vivo* data and, when compared with animal testing, our *in vitro* model provides a low-cost and high-throughput screening tool for future nanoparticle toxicity research.

Methods

Cell culture. The human colon carcinoma Caco-2 cell line and human Burkitt's lymphoma Raji B cell line were obtained from the American Type Culture Collection. The HT29-MTX cell line was kindly provided by T. Lesuffleur of INSERM U560[27]. Caco-2 cells were received at passage 17 and used in experiments at passages 30–35. HT29-MTX cells were received at passage 11 and used at passages

14–19. Caco-2 and HT29-MTX were grown in DMEM containing 4 mM Glutamax, 4.5 g l^{-1} glucose and 10% heat-inactivated fetal bovine serum (FBS). Raji cells were maintained in RPMI 1640 medium with 2 mM L-glutamine, 4.5 g l^{-1} glucose, 10 mM HEPES, 1.0 mM sodium pyruvate and 10% FBS. The cells were grown at 37 °C in 5% CO_2, and the culture medium was changed every 2 days. For experimental studies, Caco-2 and HT29-MTX were seeded at a density of 100,000 cells per cm^2 at a ratio of 3:1 Caco-2:HT29-MTX onto Transwell inserts. On day 15 of Caco-2/HT29-MTX culture, 1×10^6 Raji cells were re-suspended in 50:50 DMEM:RPMI 1640 and added to the basolateral chamber of the Caco-2/HT29-MTX culture wells. The tri-cultures were maintained for 2 days with 100 µl of culture medium replaced every day in the basolateral chamber. Raji cells were removed immediately before nanoparticle and iron transport studies. Caco-2/HT29-MTX monolayers were cultured as above except for the addition of Raji cells.

***In vivo* chicken intestinal loop studies.** Fertile Cornish-cross broiler eggs were obtained from a commercial hatchery (Moyer's Chicks) and incubated at 37 °C and 60% humidity. Twelve hatched chicks were placed in two 1 m^2 metal cages equipped with an automatic nipple drinker and manual self-feeder. Birds were kept at ~21 °C, provided with 16 h of light and given *ad libitum* access to water in a total-confinement building. During the first week post-hatch the chicks were fed a diet formulated to meet NRC recommendations[47]. Starting on day 7 post-hatch, the birds were fed a low-iron diet (51 µg Fe per g of diet; see Supplementary Table 1 for feed composition). The chickens were fed a low-iron diet to create a slight iron deficiency. This was done to maximize the amount of iron transported during the iron transport experiments. At 6 weeks of age all birds were fasted overnight. In the morning, feed intake was measured, bird weights were recorded, and the chronic exposure group ($n = 4$) was force-fed 2 mg kg^{-1} 50 nm polystyrene, carboxylated, undyed nanoparticles (Polysciences) using a plastic transfer pipette (Samco Scientific) dipped in corn oil. Birds in the chronic group were dosed with nanoparticles daily for 14 days. At 8 weeks of age, intestinal-loop iron absorption studies were performed. Birds were fasted overnight and anaesthetized with a 1 ml kg^{-1} intramuscular injection of Dial/Ketamine (Sigma Aldrich). A small incision in the lower abdomen was made to expose the duodenal loop. The duodenal loop was ligated using surgical thread (Roboz Surgical) at both ends, and a non-occlusive 22-gauge catheter was inserted into the duodenal vein. The wing vein was also exposed and a BPE-T50 polyethylene tubing (Solomon Scientific) was inserted into the vein for heparin administration to prevent coagulation in the duodenal cannula during the experiment. Initial blood samples were taken from the duodenal vein. The chronic and acute exposure birds ($n = 4$ for each treatment) were injected intraduodenally with a solution of 1 ml ^{58}Fe solution (1 mg ^{58}Fe, 92.2%, enriched, dissolved in 200 µl concentrated HCl and brought to 1 ml with 800 µl ddH_2O), 2 ml of a 10 mM ascorbic acid (pH 4) solution and 2 mg kg^{-1} 50 nm polystyrene, carboxylated, yellow-green nanoparticles. Control birds ($n = 4$) were injected intraduodenally with only ^{58}Fe and ascorbic acid. The anaesthetized birds were kept under lamps to maintain their body temperature and wetted gauze pads with warm saline were placed over the loops to maintain their moisture. Blood samples were collected before the stable isotope injection and then every 5 min for 2 h post-solution injection. A pump (ALITEA VS-10R, Precision Instrumentation) that was set to draw blood at a rate of 0.13 ml min^{-1} (total blood volume collected = 15.6 ml/2 h/bird) and 6 ml Vacutainer heparin-coated tubes were used to collect the blood samples. Samples were analysed using inductively coupled plasma mass spectrometry to determine ^{58}Fe concentrations. At the end of the procedure, an overdose of the Dial complex was used to kill the birds. Sections (5 cm) of the mid-duodenum and liver were immediately taken, and scrapings of the duodenal mucosa were isolated and stored at –80 °C in a freezer until gene expression and ferritin analysis could be carried out. RNA isolation and gene and ferritin expression analysis have been described in detail elsewhere[36] and primer sequences are listed in Supplementary Table 3. All animal protocols were approved by the Cornell University Institutional Animal Care and Use Committee.

Received 3 October 2011; accepted 6 January 2012; published online 12 February 2012

References

1. Sagalowicz, L. & Leser, M. E. Delivery systems for liquid food products. *Curr. Opin. Colloid Interface Sci.* **15,** 61–72 (2010).
2. Yoav, D. L. Milk proteins as vehicles for bioactives. *Curr. Opin. Colloid Interface Sci.* **15,** 73–83 (2010).
3. Edgar, A. Bioavailability of nanoparticles in nutrient and nutraceutical delivery. *Curr. Opin. Colloid Interface Sci.* **14,** 3–15 (2009).
4. Sozer, N. & Kokini, J. L. Nanotechnology and its applications in the food sector. *Trends Biotechnol.* **27,** 82–89 (2009).
5. Chaudhry, Q. *et al.* Applications and implications of nanotechnologies for the food sector. *Food Addit. Contam. A* **25,** 241–258 (2008).
6. Singh, R. & Lillard, J. W. Jr. Nanoparticle-based targeted drug delivery. *Exp. Mol. Pathol.* **86,** 215–223 (2009).
7. Stone, V. & Kinloch, I. *Nanotoxicology: Characterization, Dosing and Health Effects* (CRC, 2007).
8. Lomer, M. C. E., Thompson, R. P. H. & Powell, J. J. Fine and ultrafine particles of the diet: influence on the mucosal immune response and association with Crohn's disease. *Proc. Nutr. Soc.* **61,** 123–130 (2002).
9. Kerneis, S., Bogdanova, A., Kraehenbuhl, J. P. & Pringault, E. Conversion by Peyer's patch lymphocytes of human enterocytes into M cells that transport bacteria. *Science* **277,** 949–952 (1997).
10. Lomer, M. C. E., Harvey, R. S. J., Evans, S. M., Thompson, R. P. H. & Powell, J. J. Efficacy and tolerability of a low microparticle diet in a double blind, randomized, pilot study in Crohn's disease. *Eur. J. Gastroenterol. Hepatol.* **13,** 101–106 (2001).
11. Lomer, M. C. E. *et al.* Intake of dietary iron is low in patients with Crohn's disease: a case-control study. *Br. J. Nutr.* **91,** 141–148 (2004).
12. Lee, H. J. Protein drug oral delivery: the recent progress. *Arch. Pharm. Res.* **25,** 572–584 (2002).
13. Des Rieux, A., Fievez, V., Garinot, M., Schneider, Y. J. & Preat, V. Nanoparticles as potential oral delivery systems of proteins and vaccines: a mechanistic approach. *J. Control. Rel.* **116,** 1–27 (2006).
14. Galindo-Rodriguez, S. A., Allemann, E., Fessi, H. & Doelker, E. Polymeric nanoparticles for oral delivery of drugs and vaccines: a critical evaluation of *in vivo* studies. *Crit. Rev. Ther. Drug. Carrier Syst.* **22,** 419–463 (2005).
15. Ma, Y., Yeh, M., Yeh, K-Y. & Glass, J. Iron imports. V. Transport of iron through the intestinal epithelium. *Am. J. Physiol. Gastr. L.* **290,** G417–G422 (2006).
16. DeSesso, J. M. & Jacobson, C. F. Anatomical and physiological parameters affecting gastrointestinal absorption in humans and rats. *Food. Chem. Toxicol.* **39,** 209–228 (2001).
17. Muir, A. & Hopfer, U. Regional specificity of iron uptake by small intestinal brush-border membranes from normal and iron-deficient mice. *Am. J. Physiol. Gastr. L.* **248,** G376–G379 (1985).
18. Kararli, T. T. Comparison of the gastrointestinal anatomy, physiology, and biochemistry of humans and commonly used laboratory animals. *Biopharm. Drug. Dispos.* **16,** 351–380 (1995).
19. Sharp, D. G. & Beard, J. W. Size and density of polystyrene particles measured by ultracentrifugation. *J. Biol. Chem.* **185,** 247–253 (1950).
20. Whittow, G. C. *Sturkie's Avian Physiology* (Academic, 2000).
21. Barfull, A., Garriga, C., Mitjans, M. & Planas, J. M. Ontogenetic expression and regulation of Na^+-D-glucose cotransporter in jejunum of domestic chicken. *Am. J. Physiol. Gastr. L.* **282,** G559–G564 (2002).
22. Dahlke, F., Ribeiro, A. M. L., Kessler, A. M., Lima, A. R. & Maiorka, A. Effects of corn particle size and physical form of the diet on the gastrointestinal structures of broiler chickens. *Rev. Bras. Cienc. Avic.* **5,** 61–67 (2003).
23. Ojano-Dirain, C. P. *et al.* Determination of mitochondrial function and site-specific defects in electron transport in duodenal mitochondria in broilers with low and high feed efficiency. *Poultry Sci.* **83,** 1394–1403 (2004).
24. Miles, R. D., Butcher, G. D., Henry, P. R. & Littell, R. C. Effect of antibiotic growth promoters on broiler performance, intestinal growth parameters, and quantitative morphology. *Poultry Sci.* **85,** 476–485 (2006).
25. Klasing, K. C. Avian gastrointestinal anatomy and physiology. *Semin. Avian Exot. Pet* **8,** 42–50 (1999).
26. Hidalgo, I. J., Raub, T. J. & Borchardt, R. T. Characterization of the human-colon carcinoma cell-line (Caco-2) as a model system for intestinal epithelial permeability. *Gastroenterology* **96,** 736–749 (1989).
27. Lesuffleur, T., Barbat, A., Dussaulx, E. & Zweibaum, A. Growth adaptation to methotrexate of HT-29 human colon-carcinoma cells is associated with their ability to differentiate into columnar absorptive and mucus-secreting cells. *Cancer Res.* **50,** 6334–6343 (1990).
28. Mahler, G. J., Shuler, M. L. & Glahn, R. P. Characterization of Caco-2 and HT29-MTX cocultures in an *in vitro* digestion/cell culture model used to predict iron bioavailability. *J. Nutr. Biochem.* **20,** 494–502 (2009).
29. Schulte, R. *et al.* Translocation of *Yersinia enterocolitica* across reconstituted intestinal epithelial monolayers is triggered by Yersinia invasin binding to β1 integrins apically expressed on M-like cells. *Cell Microbiol.* **2,** 173–185 (2000).
30. Giannasca, P. J., Giannasca, K. T., Leichtner, A. M. & Neutra, M. R. Human intestinal M cells display the sialyl Lewis A antigen. *Infect. Immun.* **67,** 946–953 (1999).
31. Owen, R. L. & Ermak, T. H. Structural specializations for antigen uptake and processing in the digestive-tract. *Springer Semin. Immun.* **12,** 139–152 (1990).
32. Narai, A., Arai, S. & Shimizu, M. Rapid decrease in transepithelial electrical resistance of human intestinal Caco-2 cell monolayers by cytotoxic membrane perturbents. *Toxicol. In Vitro* **11,** 347–351 (1997).
33. Ranaldi, G., Marigliano, I., Vespignani, I., Perozzi, G. & Sambuy, Y. The effect of chitosan and other polycations on tight junction permeability in the human intestinal Caco-2 cell line. *J. Nutr. Biochem.* **13,** 157–167 (2002).
34. Menard, S., Cerf-Bensussan, N. & Heyman, M. Multiple facets of intestinal permeability and epithelial handling of dietary antigens. *Mucosal Immunol.* **3,** 247–259 (2010).
35. Söderholm, J. D. *et al.* Increased epithelial uptake of protein antigens in the ileum of Crohn's disease mediated by tumour necrosis factor α. *Gut* **53,** 1817–1824 (2004).
36. Tako, E., Rutzke, M. A. & Glahn, R. P. Using the domestic chicken (*Gallus gallus*) as an *in vivo* model for iron bioavailability. *Poultry Sci.* **89,** 514–521 (2010).

37. Tako, E. & Glahn, R. P. White beans provide more bioavailable iron than red beans: Studies in poultry (*Gallus gallus*) and an *in vitro* digestion/Caco-2 model. *Int. J. Vitam. Nutr. Res.* **80,** 416–429 (2010).
38. Passaniti, A. & Roth, T. F. Purification of chicken liver ferritin by two novel methods and structural comparison with horse spleen ferritin. *Biochem. J.* **258,** 413–419 (1989).
39. Mete, A. *et al.* Partial purification and characterization of ferritin from the liver and intestinal mucosa of chickens, turtledoves and mynahs. *Avian Pathol.* **34,** 430–434 (2005).
40. Tako, E., Ferket, P. R. & Uni, Z. Changes in chicken intestinal zinc exporter mRNA expression and small intestinal functionality following intra-amniotic zinc-methionine administration. *J. Nutr. Biochem.* **16,** 339–346 (2005).
41. Smirnov, A., Tako, E., Ferket, P. R. & Uni, Z. Mucin gene expression and mucin content in the chicken intestinal goblet cells are affected by *in ovo* feeding of carbohydrates. *Poultry Sci.* **85,** 669–673 (2006).
42. Caspary, W. F. Physiology and pathophysiology of intestinal absorption. *Am. J. Clin. Nutr.* **55,** 299S–308S (1992).
43. Pluske, J. R. *et al.* Maintenance of villus height and crypt depth, and enhancement of disaccharide digestion and monosaccharide absorption, in piglets fed on cows' whole milk after weaning. *Br. J. Nutr.* **76,** 409–422 (1996).
44. Tarachai, P. & Yamauchi, K. Effects of luminal nutrient absorption, intraluminal physical stimulation, and intravenous parenteral alimentation on the recovery responses of duodenal villus morphology following feed withdrawal in chickens. *Poultry Sci.* **79,** 1578–1585 (2000).
45. Basu, T. K. & Donaldson, D. Intestinal absorption in health and disease: micronutrients. *Best Pract. Res. Clin. Gastroenterol.* **17,** 957–979 (2003).
46. Hilty, F. M. *et al.* Iron from nanocompounds containing iron and zinc is highly bioavailable in rats without tissue accumulation. *Nature Nanotech.* **5,** 374–380 (2010).
47. NRC. *Nutrient Requirements of Poultry* 9th edn (National Academy Press, 1994).

Acknowledgements

The authors acknowledge financial support from the National Science Foundation for the Nanobiotechnology Center at Cornell University (ECS-9876771), the New York State Office of Science, Technology and Academic Research (for a Distinguished Professorship for M.L.S.), the Army Corp of Engineers (ID W9132T-07-2-0010) and the US Department of Agriculture. The HT29-MTX cell line was kindly contributed by Thécla Lesuffleur (INSERM U560).

Author contributions

G.J.M., M.B.E., S.D.A., R.P.G. and M.L.S. conceived and designed the experiments. G.J.M. performed the *in vitro* studies. G.J.M., M.B.E. and E.T. handled the chickens daily and E.T. and R.P.G. performed the chicken surgery. E.T. performed the microbiological analysis and M.B.E. prepared the histological samples. T.L.S. analysed the histology samples. G.J.M., M.B.E. and E.T. analysed the data. All authors co-wrote the paper.

Additional information

The authors declare no competing financial interests. Supplementary information accompanies this paper at www.nature.com/naturenanotechnology. Reprints and permission information is available online at http://www.nature.com/reprints. Correspondence and requests for materials should be addressed to M.L.S.